Space-based observations of plasma waves during conjunctions between host sensors and space objects

Lauchie Scott
Defence R&D Canada Ottawa, Canada
Paul Bernhardt
University of Alaska, Fairbanks
Andrew Howarth
University of Calgary

ABSTRACT

This study describes in-situ experimentation to measure Very Low Frequency (VLF) plasma waves (1-30 kHz) at times when a space physics satellite equipped with a radio plasma wave receiver conjuncts with other space objects to learn if a secondary space object's rapid passage near another satellite is detectable. Objects in Earth's ionosphere develop a region of ion density rarefactions in the wake of their orbital motion which could serve as the basis for object detection. In 2022 in-situ experimentation attempted detection of these ion density rarefactions as broadband VLF plasma wave noise during a space-based radio plasma sensor's rapid traversal of a secondary space object wake. This was undertaken to answer whether or not space objects are detectable by the plasma ion density disturbances that their orbital motion incurs in Earth's ionosphere. The Canadian space physics satellite CASSIOPE activated its radio plasma physics package and recorded electric field data at times prior to, during and after a known close approach was forecast between CASSIOPE and a secondary object. CASSIOPE is designed to measure Earth's aurora, particles and fields and has an eccentric 330 x 1200 km orbit which fortuitously samples a variety of plasma regimes in Earth's ionosphere. Also, for the Space Domain Awareness community, this orbit regularly crosses the altitudes of highly populated orbital shells such as Starlink, Iridium, OneWeb and other space objects offering regular conjunction opportunities to attempt measurement of plasma oscillations. Prior to a conjunction, CASSIOPE collected electric field measurements from its crossed-dipole Radio Receiver Instrument (RRI) which detects plasma electric field oscillations spanning ~1-35 kHz. In early 2022, 35 conjunctions were characterized. Four conjunctions exhibited VLF broadband noise energy spanning the ion cyclotron frequency (~36 Hz) to the Lower Hybrid Resonance frequency (~5-6 kHz) when the object passed through, or near, the secondary object's predicted wake. However, weak to strong correlation with the time of closest approach of the secondary object was found. Other conjunctions where the secondary object passed behind CASSIOPE and the RRI did not pass through the secondary object's wake did not show wave power more than the ambient background emission - consistent with the prediction that plasma outside of a space object's ion-acoustic Mach cone would exhibit undisturbed plasma behavior. While density rarefactions in a space object wake appears to be weakly associated to conjunctions in the VLF range, these findings suggest that the spatial and time separation between detected wave energy and the secondary object's motion should be examined from a plasma wave perspective where wave energy propagates relative to the geomagnetic field lines outside of the geometric constraints of a space object wake.

1. INTRODUCTION

Space-based optical detection of space objects is usually performed by detecting visual and infrared energy reflected (or emitted) from space objects. Missions such as the Space-based Visible (SBV) [1], Space Based Space Surveillance (SBSS) [2], Sapphire [3], NEOSSat [4], and ORS-5 [5] missions rely on this premise to detect space objects. These systems point optical sensors in the direction of a space object and measure sunlight reflected from their surfaces to measure their position and brightness. Space-based telescope fields of view are generally best suited to detect space objects at ranges greater than ~1000 km as the detection of space objects in their near vicinity can become problematic. A space-based observer's sensor's field of view cone apex decreases the volume of space near the observer making detection of space objects in proximity (<10 km) challenging. At these close ranges, space-based optical observers also struggle with relative angular rates >1000 arcseconds/second making trailing loss a significant factor lessening the probability of detection at close range. These considerations make the objective of optical sensing of small space objects, less than the 10 cm size limit of the Space Surveillance Network (SSN) catalog difficult to achieve.

An alternative technique to detect space objects 'close' to a space-based observer is desired. While the long-term ambition would be to detect space objects smaller than the classical catalog limit of 10 cm, this paper describes experimentation where larger, known space objects in the satellite catalog closely approach a satellite operating a plasma wave receiver to see if their passing motion is detectable as plasma oscillations. In this, we seek to answer the question: "*Can plasma waves or ion density oscillations stimulated by the motion of space objects in the ionosphere be used to infer a space object's passage near a space-based observer?*".

To answer this question, conjunctions between the Canadian CASSIOPE [6] satellite and other known space objects were analyzed using CASSIOPE's radio plasma instrument. This effort was to determine if electric field oscillations exist in the Very Low Frequency (VLF) range are measurable during conjunctions. We further analyzed specific conjunction geometries where CASSIOPE traversed the ion-acoustic wake of a secondary space object, not simply any close approach with other space objects.

This paper describes the experimental basis and setup for in-situ measurement of Very Low Frequency (VLF) radio plasma waves in, or near, the ion-acoustic wake region of space objects during conjunctions but with a focus on CASSPIOPE's motion relative to the ion-acoustic wake of the secondary space object. A description of the sensing approach, the measurement campaign, findings, and a forward-looking view toward how to improve experimentation in this nascent area of non-traditional space domain awareness sensing is presented in the sections below.

2. SPACE OBJECT WAKES

The large difference between ionospheric electron and ion thermal speeds gives rise to a wake region behind an orbiting space object [7][8]. The motion of a space object in Low Earth Orbit (LEO) at ~7.5 km/s is supersonic in comparison to typical ion thermal speed (~1 km/s) which gives rise to a negatively charged region behind a spacecraft (see Fig. 1). Electrons rapidly replenish this wake region whereas the much heavier and slower ions take longer to enter the wake to reestablish plasma neutrality. This process generates ion density rarefactions, (or enhancements) in the wake behind and orbiting space object [7][8] depending on the point of measurement downstream in the wake.

Fig. 1. shows the general wake geometry considered for this analysis relative to an object's direction of motion relative to the geomagnetic field. We use the coordinate conventions shown in Fig. 1 where the *z*-axis is aligned with a space object's orbital velocity vector $\mathbf{V_0}$ and the *x*-axis is perpendicular to the direction of space object motion. This coordinate frame is a rotation from the typical radial, in-track and cross-track (RIC) frame normally used in conjunction analysis but provides a useful basis bridging space object geophysical effects and the space situational awareness community's convention for collision assessment.
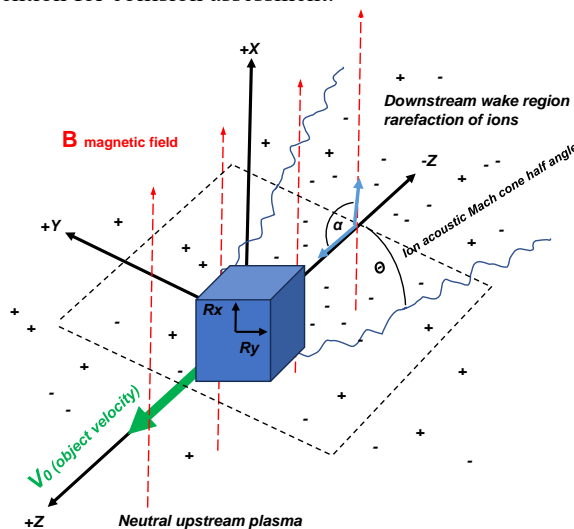
Fig. 1. Coordinate conventions and geometric definitions for a space object immersed in a plasma with a geomagnetic field. The magnetic field ($\mathbf{B}$) is in the V_0-x plane and is shown as red dashed arrows. The space object size is radius R_0. The angle of the magnetic field (α) is measured relative to the V_0 direction (90° is shown).

The magnetic field is in the V_0-x plane. The wake region of interest for this study is in the direction of –z or the anti-ram direction. The orientation angle α of the magnetic field is measured in the V_0-x plane with positive rotation about the y-axis. In Fig. 1 the motion of the space object is drawn perpendicular to the magnetic field ($\alpha=90°$) however the magnetic field can take any orientation in the V_0-x plane. If the magnetic field is aligned with the +Z axis then $\alpha=0°$. In Earth orbit the magnetic field can also project into the y-direction depending on the orbit analyzed.

Table 1 details the basic properties of ionospheric plasma in LEO at various altitudes helping to set the timescales and distance scales for this analysis. In LEO, the dominant charged particle densities arise from the electron [e-] and Oxygen [O+] species. At altitudes > 900 km or during nighttime conditions in the ionosphere, ionized Hydrogen can exceed the density of the O+ species [8]. Ion and electron temperatures are assumed to be generally equal in the ionosphere. The Debye length (λ_D) is the *e-folding* distance over which a plasma attenuates a Coulomb electric field. Earth's ionospheric plasma effectively dampens electric fields over distances less than 1 cm. In our analysis the dimensions of the space objects under study are larger than λ_D meaning that small scale electric field effects can be neglected. Similarly, the mean free path of L_e of electrons and ions is much larger than the size of space objects for altitudes above 100 km. Ionospheric plasma ions will directly impact a space object and either be absorbed, reflected or scattered off a space object's surface.

Table 1 – Properties of LEO ionospheric plasma from [7]. Bracketed values describe diurnal variation between dayside and nightside ionospheric properties.

Plasma properties	Altitude				
	100 km	400 km	500 km	700 km	1000 km
n_e (cm^{-3})	(2-100) x 10^3	(5-15) x 10^5	(4-10) x 10^5	(2-5) x 10^5	~10^5
T_i, T_n (K)	~230	1500	~1800	2000	3000
$n(O+)/n_e$	0.95 - 1	0.95 – 1	0.3 – 1	0.3 – 1	$10^{-2} – 10^{-1}$
$n(H+)/n_e$	0.02 – 0.1	0.02 – 0.1	0.1 – 0.6	0.1 – 0.6	0.5 - 1
L_e (m)	0.5	200	400	1000	8000
λ_D (cm)	1	0.2 - 0.4	0.3 - 0.6	0.4 - 0.7	1
$v_{th,e}$ (km/s)	83.5	213	233	246	301
$v_{th}[H+]$ (km/s)	1.9	5.0	5.5	5.7	7.0
$v_{th}[O+]$ (km/s)	0.5	1.2	1.4	1.4	1.8
Ω_e (1/s)	8 x 10^6	7.3 x 10^6	7 x 10^6	6.4 x 10^6	5.7 x 10^6
Ω_i (1/s)	2 x 10^2	1.8 x 10^2	1.9 x 10^2	2 x 10^2	1 x 10^3
Nomenclature					
n_e	electron density	L_e (m)	Mean free path	$v_{th}[O+]$	Thermal speed, ionized O+
T_i, T_n	ion, neutral temperature	λ_D	Debye length	Ω_e (1/s)	Electron gyrofrequency
$n(O+)/n_e$	ratio of ionized O+ to electron density	$v_{th,e}$	Thermal speed, electrons	Ω_i (1/s)	Ion gyrofrequency
$n(H+)/n_e$	ratio ionized H+ to electron density	$v_{th}[H+]$	Thermal speed, ionized H+		

The thermal velocity of particles (v_{th}) in the ionosphere is calculated using equation 1 where k_B is the Stefan Boltzman constant (1.38×10^{-23} J/K), $T_{e,i}$ is the temperature of the ion or electron in Kelvin, $m_{e,i}$ is the electron or ion density in m^{-3} and $m_{e,i}$ is the electron and ion mass in kg.

$$v_{th} = \sqrt{\frac{2 k_B T_{i,e}}{m_{e,i}}} \tag{1}$$

Two key assumptions can be made about the thermal velocity of the electrons and ion species in LEO.

1. The thermal velocity of the electrons is ~33x greater than the orbital speed of a space object. Relative to electrons, the space object is "standing still".
2. The orbital velocity of the space object is greater than the thermal velocity of the ions in LEO. For ionized oxygen, the space object orbital speed is ~5.2x greater than the thermal velocity. The space object is "supersonic" relative to ions in orbit.

Similar to aerodynamics, a satellite wake can be described as having a transitional boundary region similar to that of a Mach cone. The opening half angle θ of the cone is described as the ratio of the satellite's orbital speed to the ion acoustic speed $c_s \sim \sqrt{3k_B T_i/M_i}$ and are described as

$$M_{ion\ acoustic} = \frac{v_{orbital}}{c_s} \qquad \text{and} \qquad sin(\theta) = \frac{1}{M_{ion\ acoustic}} \qquad (2)\ (3)$$

A space object immersed in ionospheric plasma with a geomagnetic field will cause ion density rarefactions in the wake direction. In this experimentation, we model the ion rarefaction as a brief depression in ion density as a negative Dirac delta function (see Fig. 2.). Al pert [7] devised an estimate of the behaviour of the ion concentration in the wake of a space object by assuming the background plasma is Maxwellian distributed, and motion of the particles is governed by equations of continuity, momentum, and energy. The expression for magnetic field angles α not too close to zero is shown as Equation 4

$$N_i(x,y,z) = N_0 \left\{ 1 - \frac{1}{4} \left| \Phi\left(\frac{x - R_x}{zsin(\alpha) + xcos(\alpha)} \sqrt{\frac{M_i V_0^2}{2k_B T}} \right) - \Phi\left(\frac{x + R_x}{zsin(\alpha) + xcos(\alpha)} \sqrt{\frac{M_i V_0^2}{2k_B T}} \right) \right| \right.$$
$$\left. \times \left| \Phi\left(\frac{y - R_y}{2\varrho_H sin\left(\frac{\Omega z}{2V_0}\right)} \right) - \Phi\left(\frac{y + R_y}{2\varrho_H sin\left(\frac{\Omega z}{2V_0}\right)} \right) \right| \right\} \qquad (4)$$

where N_i is the spatial ion density, N_0 is the undisturbed ion concentration, Φ is the error function, α is the angle of the space object's velocity vector relative to the background magnetic field, M_i is the mass of the ion species under study, V_0 is the orbital speed of the space object (~7500 m/s), T is the temperature of the ion species, Ω is the gyrofrequency of the ion in the magnetic field, $\varrho_H = v_{th}/\Omega$ is the Lamour radius of the ions' gyro motion, x, y, z is the spatial dimensions of the distribution and R_x and R_y are the x and y spatial dimensions of the object under study. Al pert noted [7] that equation 4 does not account for thermal motion of the ions in the wake of a space object and that these density perturbations will merge back into the ambient background density on distance scales of size $z \sim 2\pi V_0^2/\Omega(kT/M_i)^{1/2}$.

Fig. 3 shows a numerical computation of equation 4 sliced in the x and y axes. The appearance of periodic ion density rarefactions behind a space object with spatial period of $z \sim 2\pi v_0/\Omega$ are visible. The other panels in Fig. 3 shows the extent of ion density rarefactions behind space objects for object motion nearly parallel to the magnetic field ($\alpha \sim 0°$), diagonally ($\alpha = 45°$) and transverse ($\alpha \sim 90°$) showing the shape of the density rarefaction waves behind a space object. The rarefactions in ion density form a narrow pulsating cone structure constrained within in the y-axis due to ion gyromotion of the particles about the magnetic field lines (see Fig. 3 left). In the x-direction the ions move parallel to the magnetic field and are not affected by the gyromotion constraint and their thermal movement governs their motion. The expansion fan of these ion density rarefactions in the x-direction depends on the size of the object relative to the gyro radius of the ions and the thermal velocity of the particles. At the altitudes of interest for this study, space objects conjuncting with the wake region should extend approximately ~1500 meters behind a space object for the O+ ion environment and ~250 meters behind an object at altitudes > 800 km. The magnitude of the ion density rarefactions varies from a fraction of a percent to ~10% depending on the orientation of the magnetic field relative to the object motion. These ion rarefactions manifest as negatively charged plasma in the wake.

If an observer were to "conjunct" through this ion density rarefaction region, the charge density can be estimated using Gauss' law by measuring the divergence of the electric field

$$\nabla \cdot \vec{E} = \frac{1}{\epsilon_0} \rho(x,y,z,t) \qquad (5)$$

where ϵ_0 is the permittivity of free space (8.854×10^{-12} C/(V·m)) and ρ is the net charge density (C/m³). Electric field perturbations due to time-spatial variation in plasma density should be detectable during a space object's passage through the wake region of another space object. Noting that the ion density rarefaction varies from 0.1-10% in Fig. 3 makes this wake region plasma slightly negative depending on the location of the observer's motion through the wake region of a conjuncting satellite. Taking Gauss's law in one dimension

$$\frac{dE}{dr} = \frac{1}{\epsilon_0} \rho(x,y,z,t) \rightarrow \frac{dE}{dt} = \frac{1}{\epsilon_0} \rho(x,y,z,t) \frac{dr}{dt} = \frac{1}{\epsilon_0} \rho(x,y,z,t) V_{rel} \qquad (6)$$

Taking for Fourier transform of both sides of the time varying electric field expression in equation (6) and assuming that the spatial density rarefaction is modelled as a negative Dirac delta function (Fig. 2), multiplying by q (electron charge (1.602x10^{-19} C) and replacing the net charge density ρ with N_0 representing the ambient electron and ion density

$$-i\omega E(\omega) = \frac{1}{\epsilon_0} V_{rel} \, \mathfrak{I}\{qN_i(t)\} \rightarrow \; E(\omega) = \frac{qV_{rel}}{-i\omega\epsilon_0} \mathfrak{I}\{N_0(-A\delta(t))\} = \frac{-iqN_0V_{rel}}{\omega\epsilon_0} (\, A(1) \,) \qquad (7)$$

The complex power of equation 7 indicates that broadband electric field oscillations should be observed proportional to the magnitude of rarefaction percentage A and the relative velocity of the objects V_{rel} during an observer's motion through the negative wake of a space object during a conjunction. The power should exhibit a "fall off" inversely proportional to the angular frequency $\sim 1/\omega$. The absolute magnitude of 7 is

$$|E(\omega)|^2 = \frac{(qN_0V_{rel})^2}{\epsilon_0^2} \frac{A^2}{\omega^2} \quad [\text{V}^2/\text{m}^2] \qquad (8)$$

At the altitudes of this study, at average orbital speeds of ~7.5 km/s, and a 1% ion density rarefaction in the wake of a space object should generate broadband electric field amplitudes on the order of ~8 V/m at 1 kHz, ~1.4 V/m at 6 kHz and ~0.8 V/m at 10 kHz.
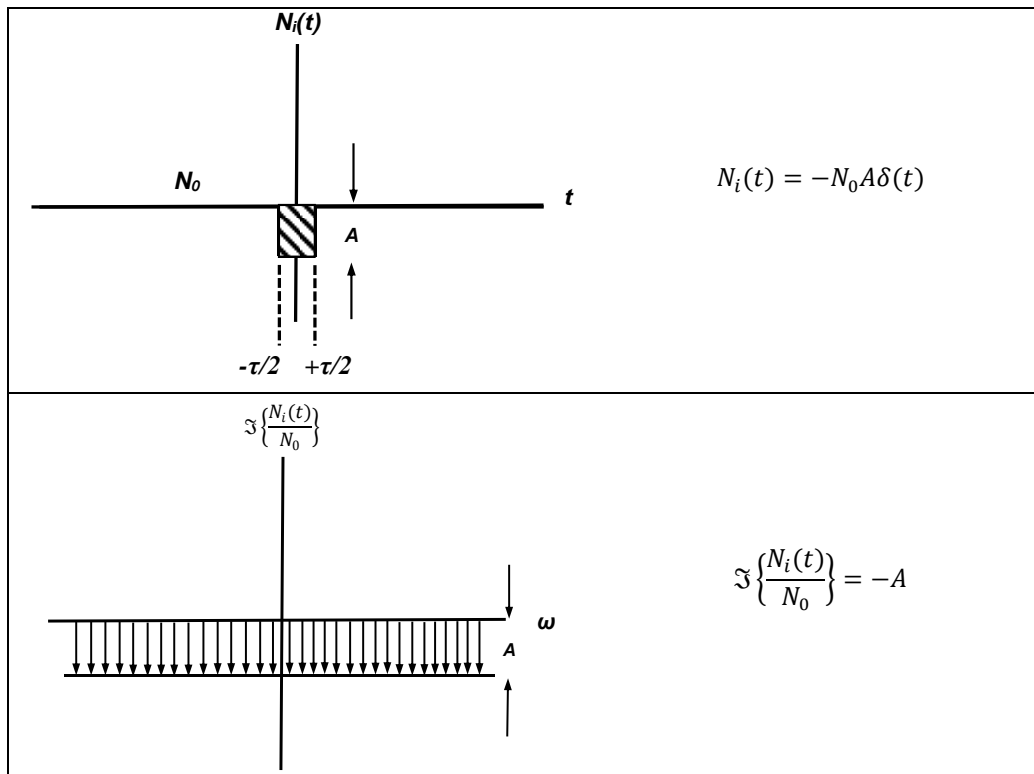

Fig. 2. Ion density rarefaction pulse as observed by a transiting satellite. *Top*: Density and time profile of the observer transiting a sudden ion density rarefaction where the plasma has a net charge of zero, then a sudden negative pulse in plasma density is observed. *Bottom*: broadband frequency response to a space object quickly transiting the wake of another space object.

α = 0° (motion parallel to magnetic field)

α = 45°

α ~ 90° (motion perpendicular to magnetic field)
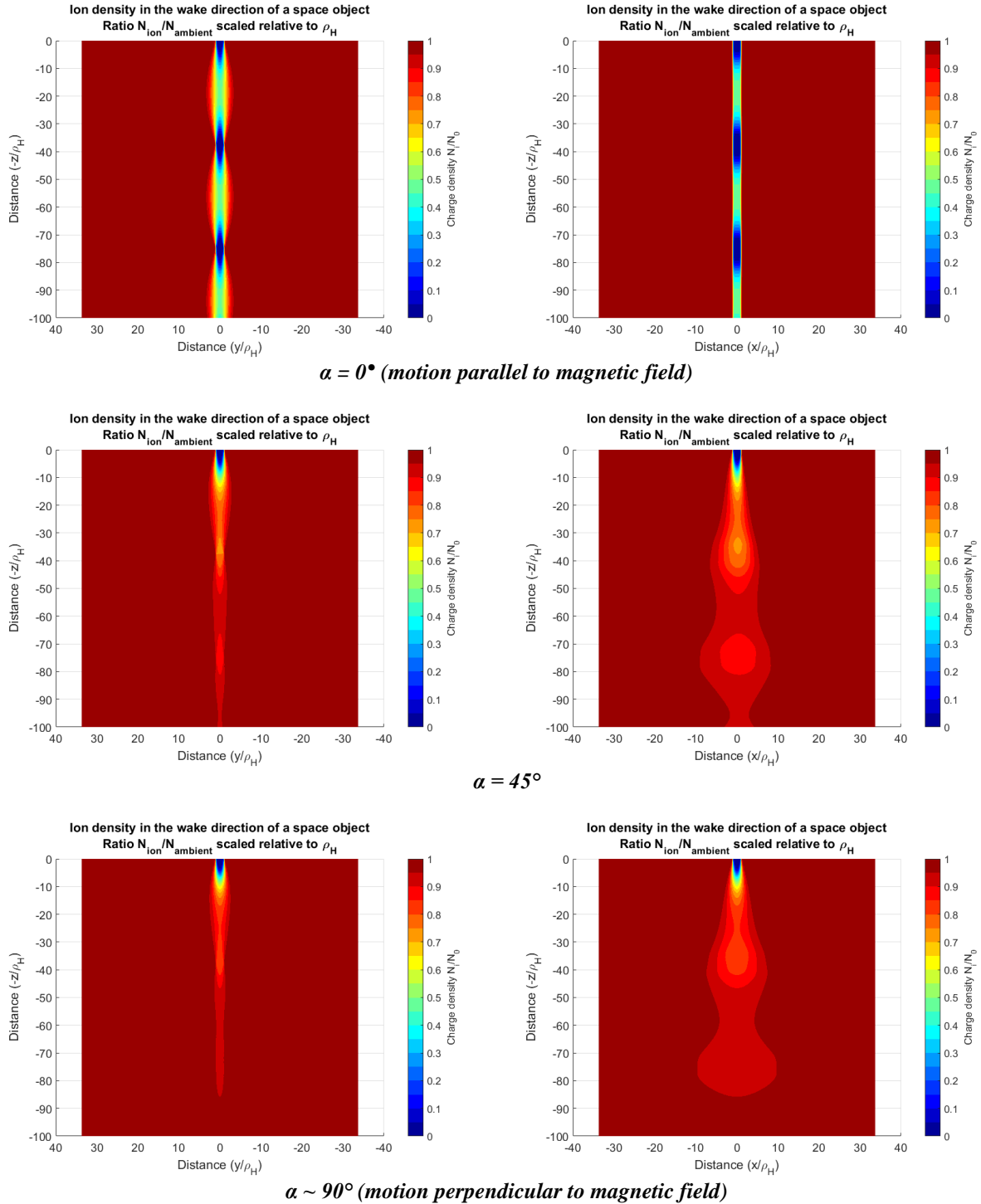
Fig. 3. Ion density rarefactions in the wake of a space object. The object is at the top of all plots at (0,0) and shows a sharply negative plasma region directly behind the space object. The wake dimensions are scaled relative to the Larmour gyroradius ϱ_H of the ions for various geomagnetic field angles α. The object has dimensions in the *x* and *y* directions the same size as ϱ_H. (*Left*): Density rarefactions in V_0-y plane which constrain the ion motion due to Lorentz gyromotion due to the magnetic field forming a narrow wake in this plane. Periodic variations in density are visible in the -*z* direction. (*Right*): Ion density rarefactions in V_0-x plane showing the periodic structure in ion density rarefactions extending in a broadened fan-like manner.
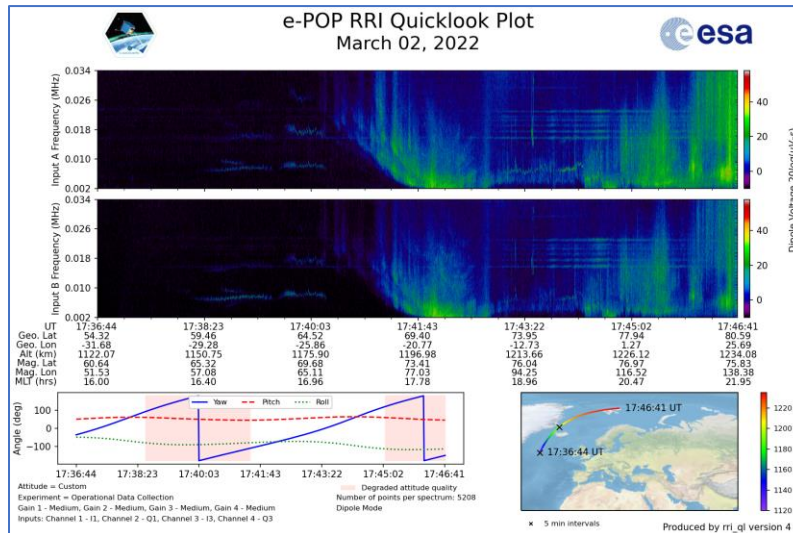
3. CASSIOPE

The **CAS**cade, **S**mallsat and **IO**nospheric **P**olar **E**xplorer (CASSIOPE) is a Canadian space-physics mission (see Fig.4.) launched in September 2013 to perform measurements of Earth's geospace environment using its e-POP space physics package [6]. CASSIOPE is in a 330 x 1150 km orbit (as of 2023) at 81° inclination and registered with a COSPAR identification as 2013-055A. CASSIOPE at is operated by the University of Calgary with Earth stations in Kiruna (Sweden), Inuvik (Canada), and O'Higgins (Antarctica). The instruments aboard CASSIOPE enable ionospheric and auroral research by collecting magnetic, electric field, GPS signal strength, near infrared optical[1], and ion data. CASSIOPE's last reaction wheel ceased functioning in 2021 and is now in a Sun-aligned spin which keeps sunlight on its main solar panel. CASSIOPE now relies on star tracker inputs for attitude estimation and its magnetorquers for coarse attitude control of its yaw spin rate of ~1 °/s. This spin rate enables some e-POP science instruments to continue data collection despite CASSIOPE's diminished attitude control state.
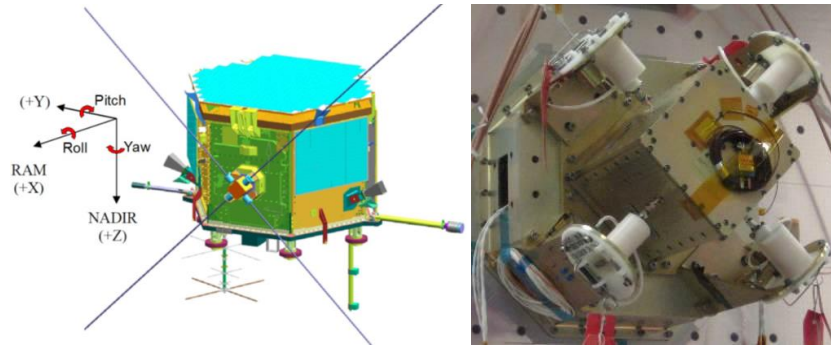
Fig. 4. *Left:* CASSIOPE satellite with its four monopole antennas deployed. *Right:* RRI with antennas stowed. Image credits: University of Calgary [10]

Measurements of electric field oscillations is achieved using CASSIOPE's Radio Receiver Instrument (RRI). The RRI was designed to measure the morphology and dynamics of ionospheric F-region density structures, auroral wave-particle interactions and backscatter [9]. The RRI uses four monopole antennas which measure electric field strength

Fig. 5. Sample electric fields spectrogram from CASSIOPE's RRI during a pass through the auroral region near 70° north latitude. Image credits: University of Calgary [10].

---

[1] The Fast Auroral Imager (FAI) has seen regular use by Canadian researchers as a wide field space domain awareness sensor for detecting megaconstellation objects in the past 4 years.

on a variety of channels and bandwidths. These antennas can be operated as individual monopoles or as dipoles (see Fig. 4. Left). The antennas are each 3 m long which measure electric fields from 1 µV/m to 1 V/m at a sample rate of 62,500 samples per second. The RRI can measure electric field frequencies spanning 10 Hz to 18 MHz. The crossed dipole arrangement provides 2-dimensionsional polarization insight such that wave direction can be inferred. A spectrogram of detected electric field data based on the in-phase and quadrature measurements from the antennas working in dipole mode is shown in Fig. 5 where CASSIOPE was traversing the auroral and observing significant very low frequency (VLF) energy while transiting the auroral region. Given that CASSIOPE would see electric field strengths exceeding 1 V/m at frequencies less than 6 kHz, it is expected that the RRI would saturate at lower frequencies if a wake traversal were to occur.

4. EXPERIMENT PLANNING

Planning this collection campaign required unusually low overhead and infrastructure. Initially *any* conjunction was planned for RRI data collection by finding CASSIOPE conjunctions from the Celestrak SOCRATES [11] website. SOCRATES' screening volume is somewhat larger than the 19th Space Control Squadron's screening criteria which enabled rapid planning of RRI data collects early in this effort. This also enabled a "what-if" testing to see if the RRI could detect objects, or other phenomenology, at longer ranges. Conjunction Data Messages (CDMs) were also employed and served as another data source but reflected space objects conjuncting with CASSIOPE within the CDM 0.4 km radial, 44 km in-track and 51 km cross-track screening volume [12]. These conjunctions provide 2-3 days of lead time prior to the conjunction for commands to be sent to CASSIOPE's RRI instrument to begin recording electric field measurements centered on the Time of Closest Approach (TCA). For each conjunction planned either using SOCRATES or the 18th's CDM service, a 2-minute data collection centered on the conjunction's TCA was programed aboard CASSIOPE's computer. Commands for RRI data recording was generally uploaded a day or so before the conjunction event during one of CASSIOPE's daily ground station passes.

In addition to either SOCRATES or 19th CDM messages, a further criterion was applied where a 6 km long conical region behind the secondary object's $-V_0$ direction was added. A 10° half angle conical region would test if CASSIOPE would traverse the area in the space object wake (see Fig. 6). This conical region represents an approximation of the ion acoustic Mach cone geometry. This screening criteria significantly reduced the number of conjunctions as the ion acoustic Mach cone is a more restrictive screening volume compared to either SOCRATES or the 19th's volume screening criteria.
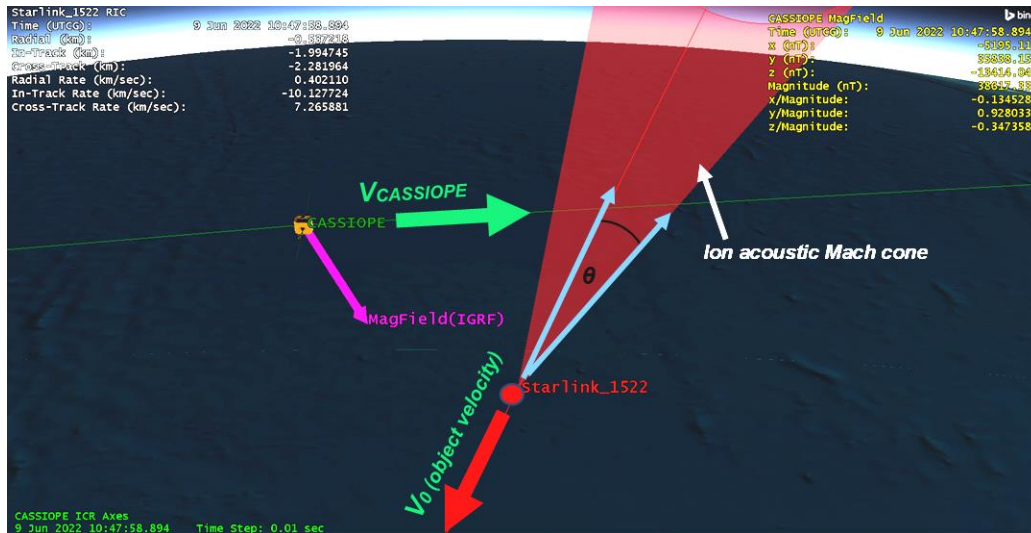
Fig. 6. Geometry for a conjunction where the motion of CASSIOPE passes through the ion-acoustic Mach cone of the secondary space object in LEO.

CASSIOPE's RRI was set to acquire VLF range data at a sampling rate of 62500.33933 Hz. If CASSIOPE were to transit an ion depleted region of ~1 ion gyroradius (~5 meters) width at an average speed of 7.5 km/s the RRI would acquire approximately 41 electric field samples during its traversal. VLF frequencies in the 10 Hz to 36 kHz regime

was chosen for this experimentation due to the likelihood of higher broadband power at lower frequencies. An +18 kHz offset to spectrogram data collected in the VLF range is applied when operating the RRI to correct its collection bandwidth to the frequency range being measured [9]. After the conjunction CASSIOPE's RRI data is downloaded approximately two days later and processed into spectrograms by the University of Calgary's e-POP data server[2]. At this stage, the data is further analyzed for the presence of wave energy prior to, during, and after the conjunction. RRI data is also available for analysis with separate applications by downloading h5-formatted binary files [10] available from the University of Calgary e-POP data server.

5. MEASUREMENTS AND RESULTS

From March to June 2022, 35 conjunctions were sampled using the RRI. Annex 1 details the space objects which had close approaches with CASSIOPE and RRI data collected. It should be noted that a variety of miss distances and close approach trajectories were attempted in this timeframe to determine if wave effects could be correlated with the secondary object's passing. Many conjunctions acquired data at very large distances to determine if effects, other than wake density rarefaction effects, could be measured.

Fig. 7a-7c shows the distribution of radial, in-track and cross-track miss distances and the altitudes that the conjunctions were observed by CASSIOPE. It is notable that a large portion of the conjunctions occur at ~550 km and 800 km altitudes reflecting the two most heavily populated orbital shells in LEO. Other conjunctions above 1000 km is likely to have encountered plasmaspheric ions (primarily H+) where the wake region is likely to be very short behind the space object. Fig. 7d shows that most of the conjunctions occurred at mid-latitudes or higher suggesting the magnetic field was relatively perpendicular to the direction of space object motion at TCA.
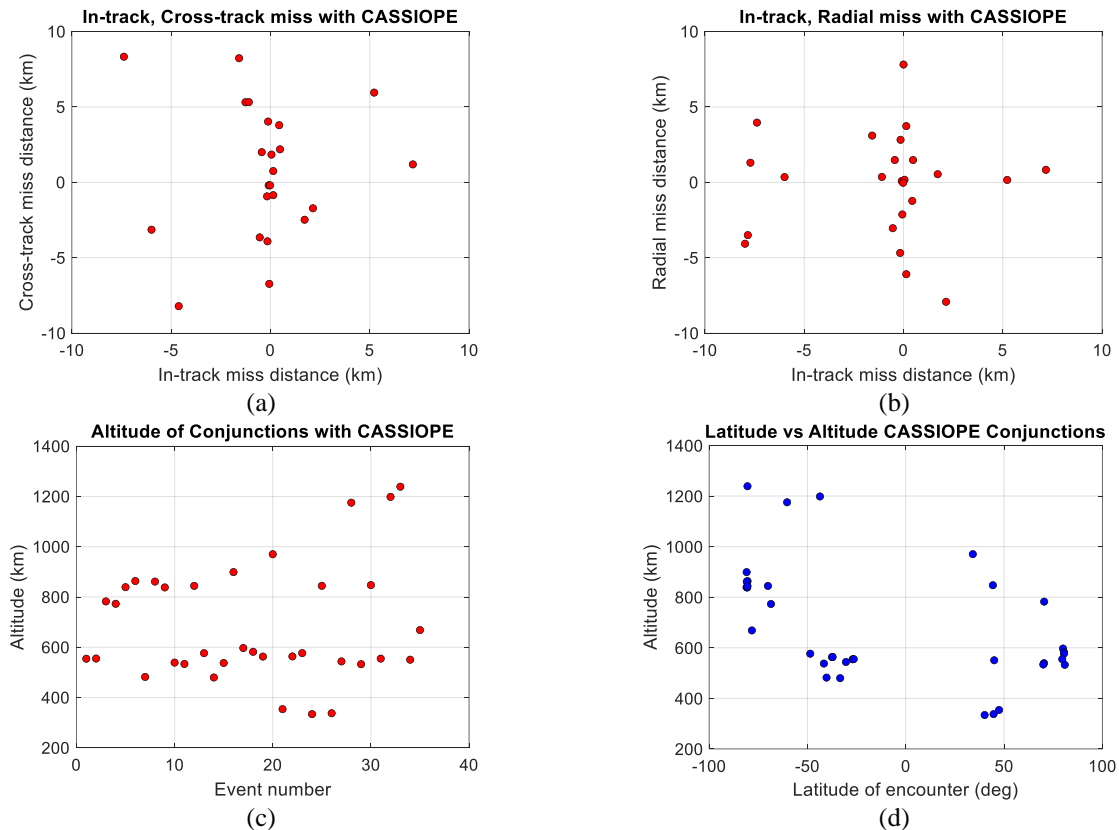

Fig. 7. (a) In-track, cross-track miss of space objects relative to CASSIOPE (b) Radial, in-track miss distances (c) altitude of the conjunctions (d) latitude-altitude plot.

Fig. 8 shows an example spectrogram of CASSIOPE RRI channel A and channel B electric field measurements collected from the dipoles during a very distant pass of a Starlink satellite (~95 km) which served as a calibration reference where no ion density rarefaction should have been detected. The spectrograms were processed over the frequency range of 200 Hz – 36 kHz. The conjunction is demarcated by a vertical white line which indicates the conjunction TCA.

Artificial and natural noise sources are identifiable in Fig. 8. Ground-based VLF transmitters are visible as horizontal constant "tones" at 16, 18, 20, 22, 24, 25 kHz. These frequencies are often used for subsurface naval communications and time reference. Below 10 kHz several natural ionospheric "whistlers" [13] are visible where terrestrial lighting impulses travel along Earth's magnetic field lines, reflect at the ionosphere boundary and travel backward to the conjugate ionospheric boundary. Whistlers last for 1-2 seconds and the velocity of the low frequency waves travel slower than the high frequencies. This creates a whistler's unique "descending-whistle" tone when played as a sound. "Nose whistlers" are also shown where lightning directly couples from the ground to space and has broadband power above 6 kHz. It is also notable that in CASSIOPE's Channel B (Fig. 8 lower plot) whistlers and other noise sources are stronger in this polarization suggesting the CASSIOPE's dipoles 3 and 4 were more aligned with the waves' polarization at the time of measurement. No wave energy is attributed to the passing Starlink satellite in this plot as the separation between CASSIOPE and the passing Starlink was ~95 km.
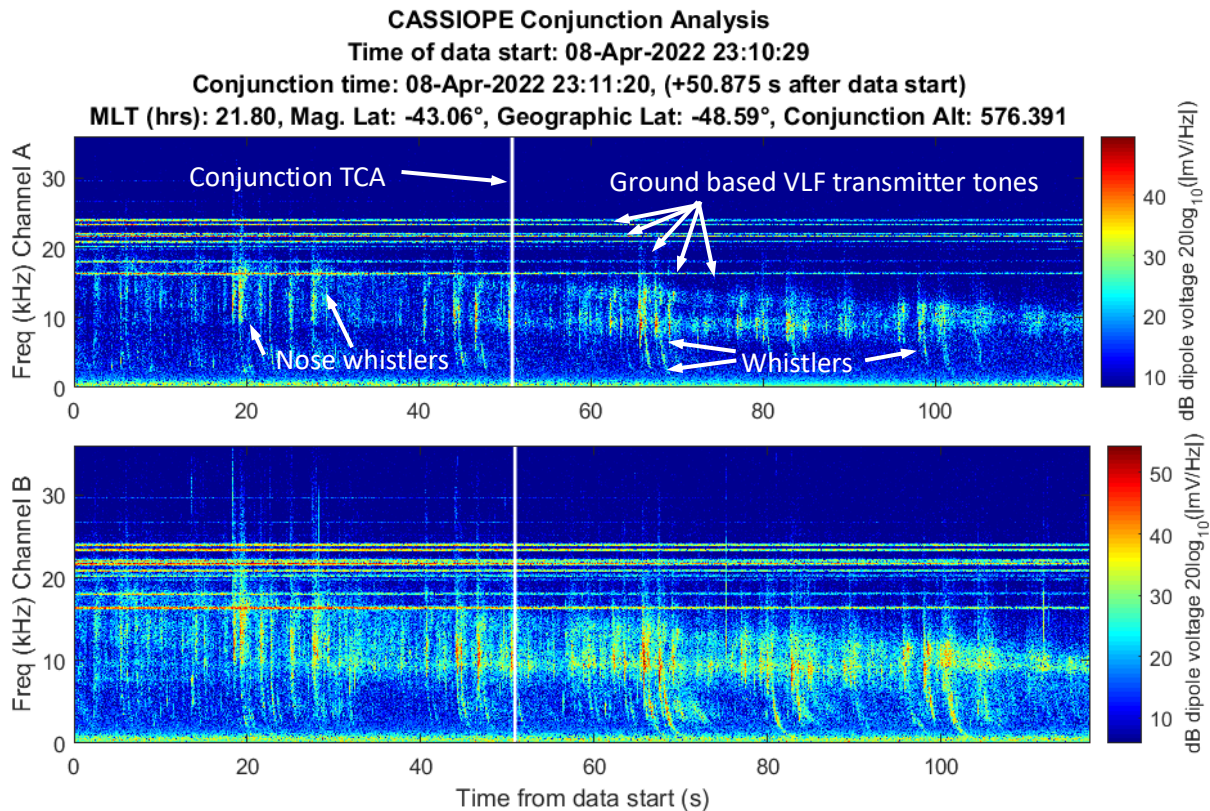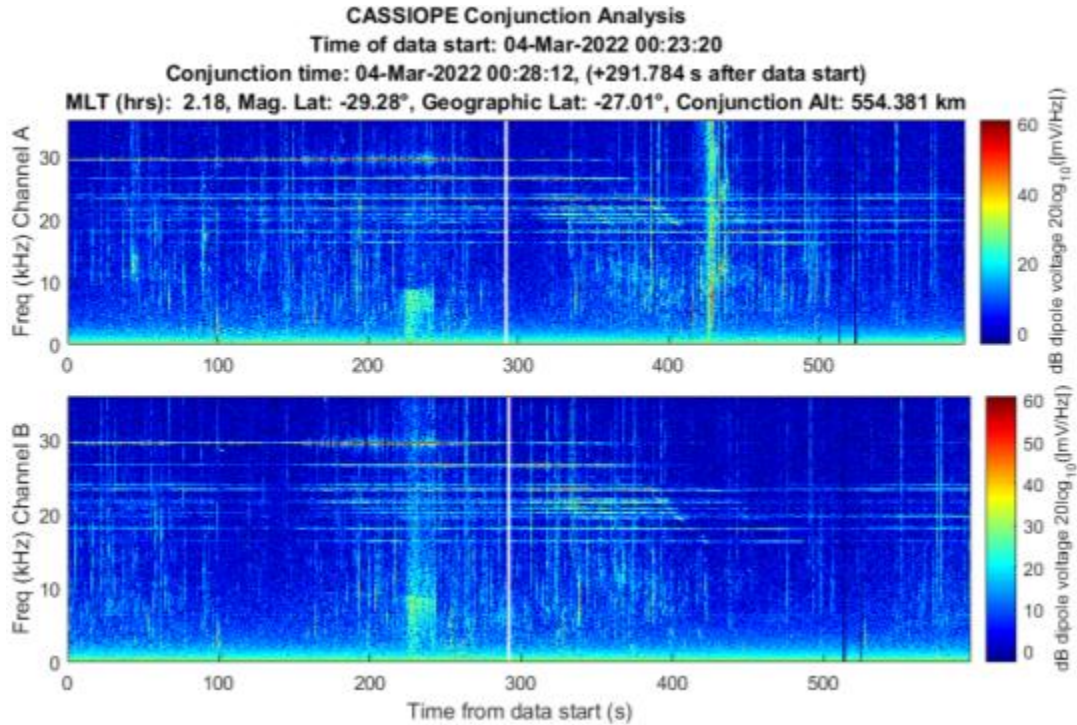

Fig. 8. Spectrogram of detected VLF electric fields recorded by CASSIOPE's RRI dipoles Channel A: dipoles 1,2 and Channel B: dipoles 3,4 during a distant pass between CASSIOPE and Starlink 2572 (miss distance was ~95 km). It was not expected to see any detectable signal from the Starlink during the passage and representative artificial and natural noise sources are indicated.

Starlink 2672

Starlink 2672 was predicted to miss CASSIOPE by 17.7 km with an in-track miss distance of -7.71 km. Starlink 2672 was predicted to pass well behind CASSIOPE and it would not pass through Starlink's wake. The RRI was activated anyway, and the results are shown as Fig. 9. Some broadband energy at lower frequencies was detected, but nearly 63

)

seconds prior to TCA and appears at the 229 second mark in Fig. 9. Channel B appears to show more wave energy in that polarization. The energy appears to be "capped" by the Lower Hybrid Resonance frequency (LHR) which is the hybrid between the plasma frequency and the electron cyclotron frequency. An examination of the satellite catalog at the time of the burst did not show other space objects in the immediate vicinity or threaded along the magnetic field vector. It is not known if the electric propulsion system was active on Starlink 2672 at the time that the RRI was recording its data. A nose whistler appears as the 420 s mark and does not appear correlated with the conjunction.


CASSIOPE Conjunction Analysis
Time of data start: 04-Mar-2022 00:23:20
Conjunction time: 04-Mar-2022 00:28:12, (+291.784 s after data start)
MLT (hrs): 2.18, Mag. Lat: -29.28°, Geographic Lat: -27.01°, Conjunction Alt: 554.381 km

Fig. 9. Spectrogram of CASSIOPE's conjunction with Starlink 2672. Miss distance of 17.7 km. Note that a broadband burst of energy at low frequencies is detected, but ~63 s "earlier" than the expected time of conjunction.
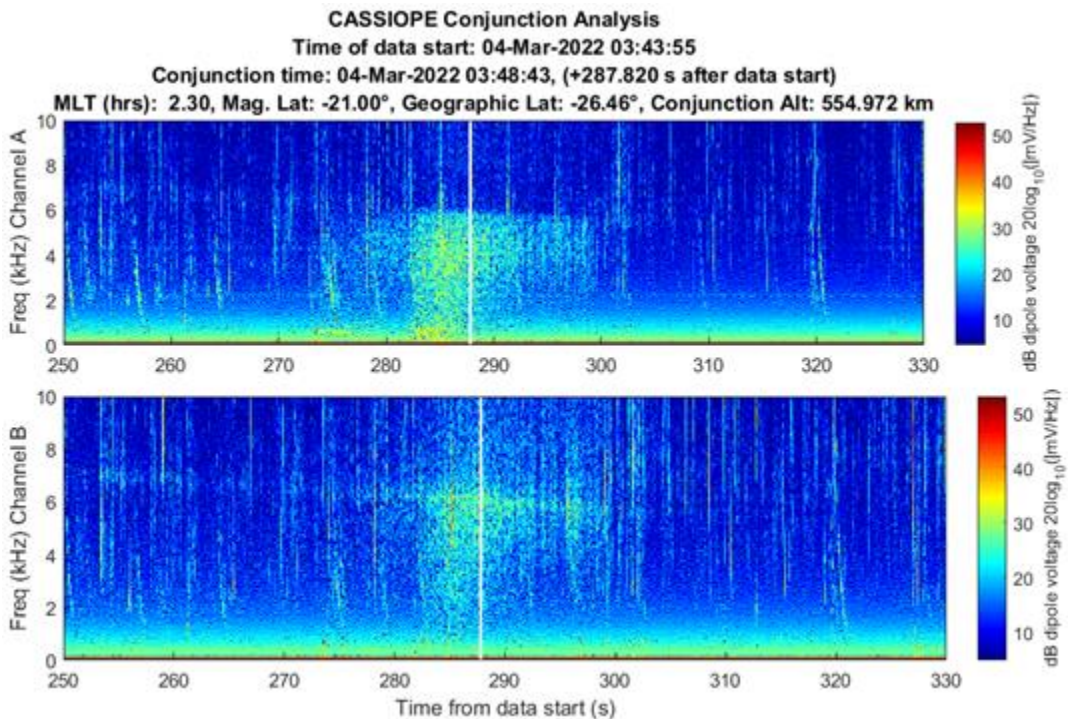
Starlink 2521

Starlink 2521 was predicted to miss CASSIOPE by 0.24 km with an in-track miss distance of –0.090 km based on the publicly available orbital catalog data. CASSIOPE was predicted to pass ahead of Starlink 2521 during a night-side pass between the two objects. RRI data for this close approach is shown in Fig. 10. Broadband energy at frequencies less than 10 kHz was detected centered on the conjunction and with most power at the LHR. Channel B appears to show more wave energy in that polarization. A communication with SpaceX [14] indicated that the Starlink 2521 was not using its electric propulsion system at the time this RRI data was recorded.

The burst of power is emphasized in a zoomed in plot in Fig. 11 but appears to be "capped" by the LHR of ~ 6 kHz at the time on conjunction. There is a strong pulse of power about 3 seconds prior to TCA. The time width of the pulse is ~17 seconds wide which is wider than anticipated for a broadband noise spike. While well correlated in time for the conjunction, and well matched in terms of the proximity of Starlink 2521 with CASSIOPE, it appears that other dynamics was driving the broadband power during this conjunction.
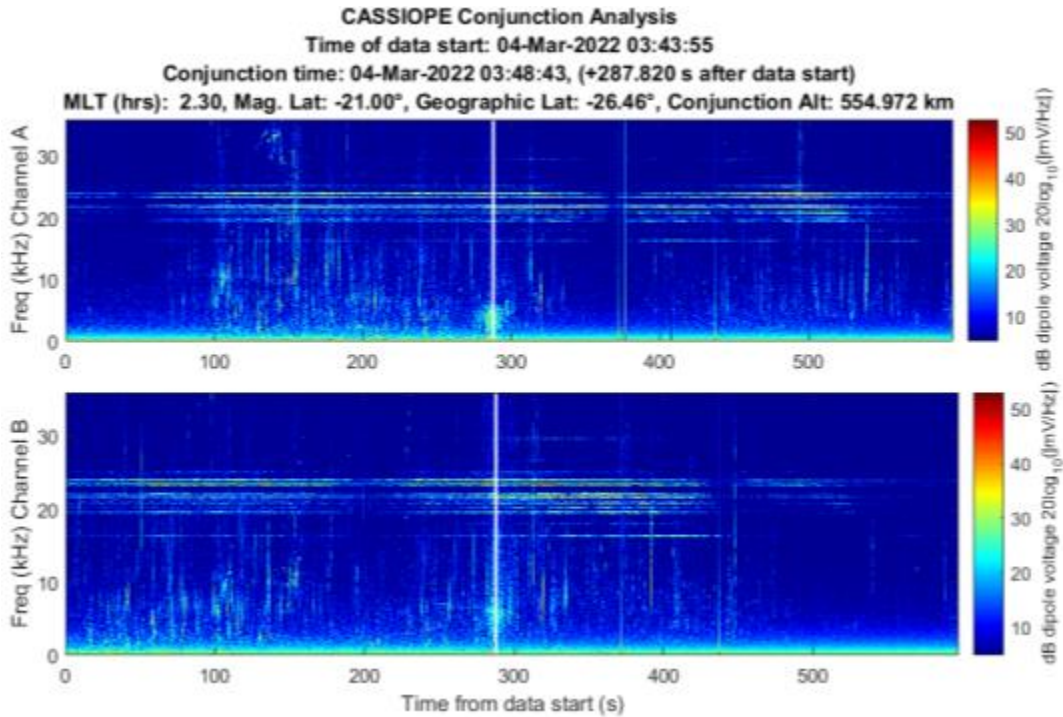
Fig. 10. Spectrogram of detected VLF electric fields during CASSIOPE's conjunction with Starlink 2521 on 4 Mar 2022. Miss distance of 0.24 km. A broadband burst of power at low frequencies is observed centered on the TCA of the conjunction but does not show much power at frequencies above the LHR (~ 6 kHz).

Fig. 11. Spectrogram of detected VLF electric fields during CASSIOPE's conjunction with Starlink 2521 with an emphasis on the time of conjunction and showing power below 10 kHz frequencies.

Given the close approach between the two objects, further orbital analysis was performed. CASSIOPE's GPS reference ephemeris was obtained yielding ~5 meter precision in its orbital position. Supplemental TLEs available from Celestrak [11] for the Starlink satellite were used to further refine its orbital position as reference ephemerides were not available. These supplemental TLEs which are "fitted" on Starlink operator ephemeris are generally precise to ~240 meters at epoch for a Starlink satellite that is not maneuvering. This refined orbital data indicated that Starlink 2521 flew somewhat above CASSIOPE by 311 meters, but the geomagnetic field vector which extended through CASSIOPE "threaded" Starlink 2521's wake during conjunction (see Fig. 12.). This geometry suggests that electrostatic noise [15][16] may be the cause of this effect, and not the ion density rarefaction that was envisaged for this experiment. Section 8 describes the historical basis of this effect where other space missions have observed broadband noise from the wake of other space objects.
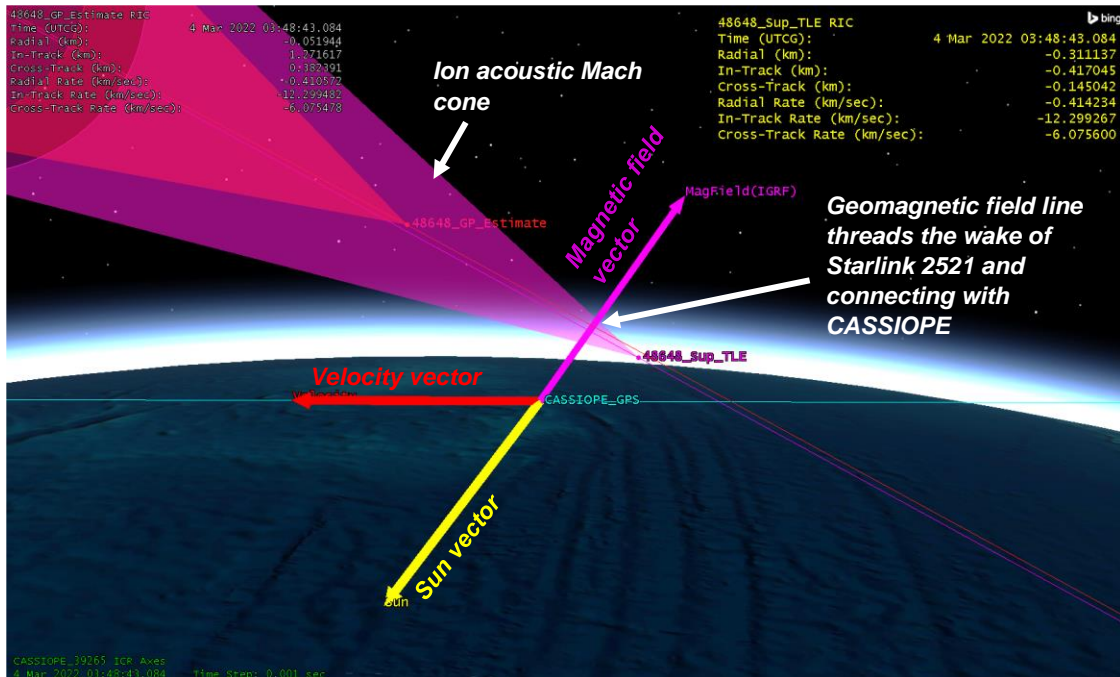

Fig. 12. Geometry of the conjunction between CASSIOPE and Starlink 2521. The supplemental TLEs available from Celestrak [11] are ~2 km further in-track compared to the elset available from the satellite catalog. The geomagnetic field vector "threaded" the wake region when the objects were separated by -417 m in the in-track direction.
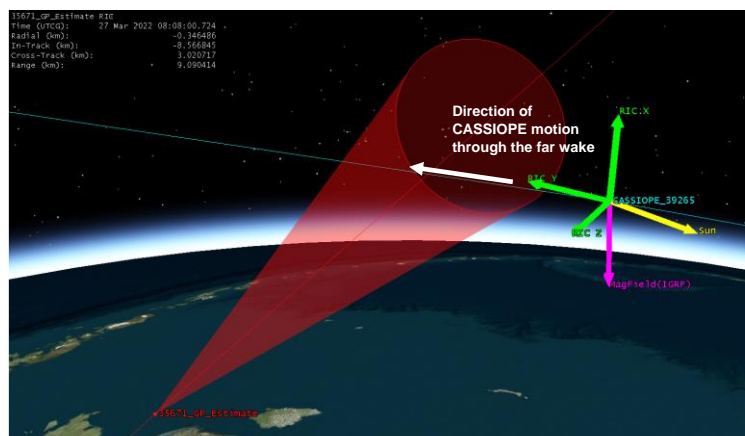

COSMOS 2251 Debris

A piece of COSMOS 2251 debris was predicted to miss CASSIOPE by 7.92 km with an in-track miss distance of 5.95 km. RRI data is shown in Fig. 13. CASSIOPE entered the conical wake region nearly 10 km behind the debris object (See Fig. 15). Broadband energy at frequencies less than 10 kHz did appear, but the proximity of the conjunction near the auroral oval (~70° latitude) where natural currents from Earth's magnetosphere complicates the differentiation of this wave energy from the passing object. Channel B's polarization also shows power below 6 kHz and is emphasized in Fig. 14 centered on the TCA of the conjunction. As this conjunction occurred within the auroral oval latitudes the energy observed on Channel B may be originating from the magnetosphere however it is correlated with the TCA. Some VLF energy below 6 kHz is visible but occurs ~3 seconds prior to the conjunction and approximately 16 seconds afterward.
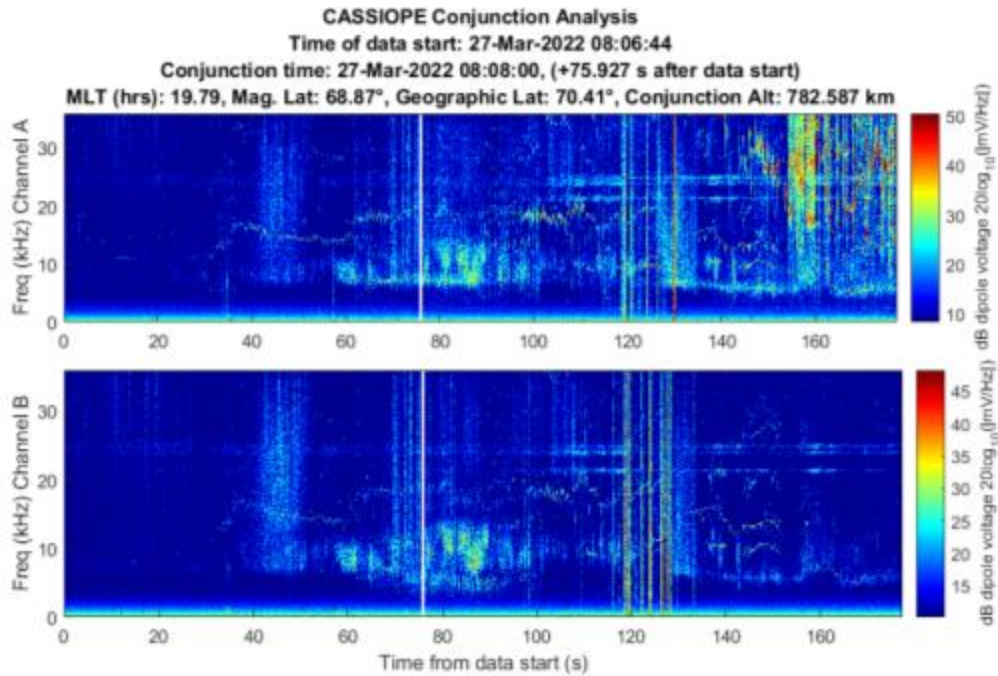
Fig. 13. Spectrogram of detected VLF electric fields during CASSIOPE's conjunction with COSMOS 2251 debris
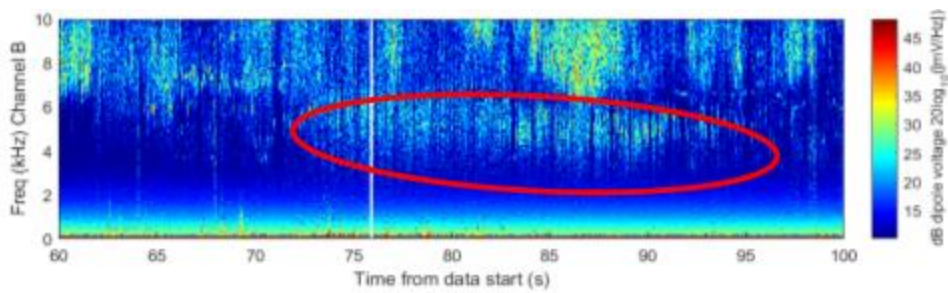
Fig. 14. Spectrogram of detected VLF electric fields during CASSIOPE's conjunction with COSMOS 2251 debris emphasizing Channel B energy detected under 10 kHz. A burst of power is visible from 4-6 kHz.


Fig. 15. Motion of CASSIOPE toward the wake region of the COSMOS 2251 debris. CASSIOPE's pass is well behind the debris object and rapidly traverses the far wake.

Iridium 911

CASSIOPE had a close approach with Iridium 911 with a miss distance of 7.32 km with an in-track miss distance of 7.17 km. RRI data is shown in Fig. 16. Power above 6 kHz is visible but the location of the conjunction near the southern auroral region makes it difficult to fully attribute the passage of the Iridium satellite. Significant energy is visible in Channel A which appears to be due to auroral particle precipitation. This conjunction was interesting in that CASSIOPE's orbit was nearly parallel with the direction of motion of Iridium 911 and CASSIOPE took a full 2 seconds to traverse the 10° conical region behind the space object. CASSIOPE averaged ~7 km behind Iridium 911 during its 2 second passage though the extended wake region.
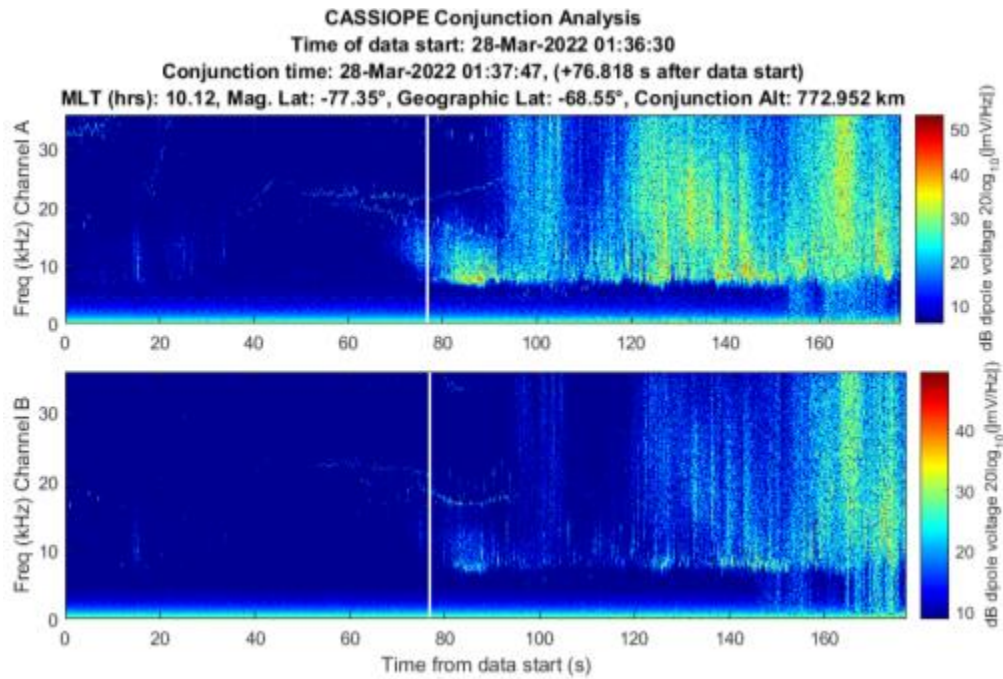
Fig. 16. Spectrogram of detected VLF electric fields during CASSIOPE's conjunction with Iridium 911
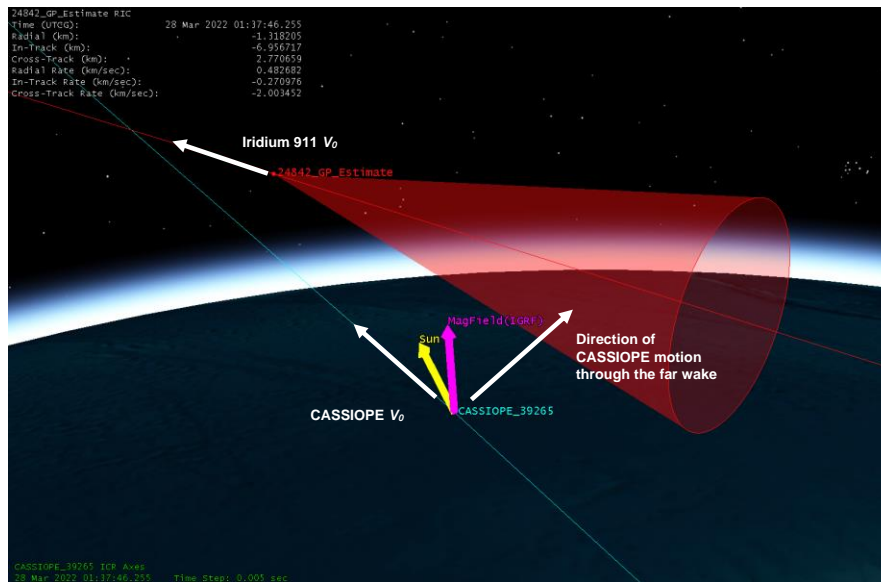
Fig. 17. CASSIOPE's motion relative to Iridium 911 showing its trajectory through the far wake of Iridium 911

Other Conjunctions

The other 31 conjunctions analyzed in this dataset did not show low frequency power appearing to correlate anywhere in time with the conjunction TCA. This is largely attributed to these conjunctions' larger stand-off distances or relative motion well ahead of wake region of the space object. The features observed in the first 2 Starlinks did not reappear during other Starlink passes observed in the dataset. Annex 1 details the summary findings for these observations indicating if broadband power was observed near the TCA for the conjunction. Commentary on the presence of whistlers, audible voice recordings from VLF broadcasts, data interruptions and other phenomenology are noted.

6. INTERPRETATION

The conjunction geometry required for this experimentation was very challenging and very constraining for planning. Conjunctions where CASSIOPE passes through the ion acoustic wake of another space object are rare despite the generally high frequency of conjunctions in LEO. Given that most objects passed many kilometers from CASSIOPE, the data collected in this initial campaign makes it difficult to conclusively say whether sensing a space object by detecting the ion depletion or enhancements behind the moving space object is possible. More data is currently being acquired and this work represents a first initial attempt at sensing known space objects by looking for electric field oscillations in the background plasma environment. Electric field strengths detected during the four most promising conjunctions did not show fields anywhere near the 1 V/m expectation for wake traversals. The detected field strengths were closer to ~ 1 mV/m which is more consistent with the behavior of electrostatic noise [15].

The data acquired on Starlink 2672 and Starlink 2521 showed some indication that broadband energy detection may be detectable, but the lack of repeatability of the conjunction geometry and the significant time offset of Starlink 2672 makes these results inconclusive. The results do reinforce the prediction that the size scale of the ion depletion region "merging" back into the ambient density environment should do so at a distance of $z \sim 2\pi V_0^2 / \Omega (kT/M_i)^{1/2}$ for both species of dominant ions (O+ and H+). Above 300 km altitude, this would be in-track distance scales of the ion acoustic wake of ~ 1.7 km for O+ and 0.03 km for H+. This suggests this experimentation should focus on the LEO environment below 800 km where O+ is the dominant ion where wake traversals are more likely to occur. This experimentation should also focus on collections on the dayside of the Earth where the diurnal O+ ionospheric density exceeds that of H+. The broadband power fall-off expected from equation 8 was not exhibited in the Starlink 2571 data and may be simply because the refined orbital position of Starlink 2571 showed that it did not enter the wake region but rather the geomagnetic field "threaded" the Starlink's wake. This may be indicative of LHR plasma wave noise which is known to follow geomagnetic field lines (see section 8)

The VLF noise environment posed challenges to disentangle VLF signals from nearby space objects in space. Artificial noise sources from ground-based VLF transmitters tend to operate above 15 kHz and their steady predictable tones do not appear to offer a great challenge when inspecting spectrograms for broadband VLF noise. However, the natural VLF environment comprised of whistlers and other auroral noise does generate considerable power in the frequency ranges expected for this experimentation.

Geometric complexity of the wake plays a role as well, the wake of a space object tends to broaden in the *x*-direction when the space object's motion is perpendicular to the geomagnetic field. Therefore, it is more likely to cross the wake when conjuncting with space objects at higher magnetic latitude. This is tempered by the fact that the auroral regions near +/- 70° latitude strongly precipitate particles which could overwhelm subtle electric field measurements. The auroral regions, which tend to have a promising velocity-magnetic field geometry, pose a challenge to observe subtle ion density depletions behind a space object due to high natural auroral electron currents.

7. RECOMMENDATIONS

Upon analysis of the RRI data, and assessment of the geometric and other space physics constraints for attempting to detect ion depletion regions in the wake of a space object, the following recommendations are made:

1. **Altitude:** The conjunction should be planned for altitudes less than 800 km which help ensure that O+ is the dominant ion species. The heavier ion mass of O+ increases the effective length of the wake before the density depletions merge back into the ambient ion density environment due to natural thermal motion of the ions.

2. **Dayside conjunctions:** Dayside ionospheric plasma is predominantly O+. Conjunctions where VLF data is collected should occur when the spacecraft and the ambient ionospheric plasma are dayside illuminated is recommended. This helps ensure the wake region is extended to help increase the likelihood of its traversal.

3. **Conjunction planning:** While TLEs were used as the primary method to compute the TCA for the conjunction and the motion relative to the wake, the use of CDMs from the 19th Space Control Squadron are recommended for increased orbital planning precision. CDMs also contain useful ancillary data regarding the orbital uncertainties of the objects and the estimated radar cross section (size) of the secondary object. Alternatively, TLEs based on the operator ephemeris, such as the supplemental TLE available from Celestrak [11] can offer a better degree of precision for some constellations which publish operator ephemeris.

4. **Mach cone constraint:** The original planning for this experimentation used "any" conjunction to plan RRI data acquisition. A further constraint where a ~7-10° half cone angle representing the Mach cone should be computed to validate if the sensor passes through the Mach cone. The extent of the Mach cone should not exceed ~ 2 km in the wake direction of the space object.

5. **Latitude:** The auroral regions near +/- 70° north and south latitude which have an extent of ~6-10° across should be avoided due to the likelihood of high background noise from magnetospheric currents in this region. Geomagnetic storms may further degrade acquisition effectiveness thus geomagnetically quiet conditions may be preferable for this research.

6. **Magnetic field measurements:** Electric field measurements were collected during this initial experimentation with CASSIOPE. It is recommended to collect magnetic field measurements to search for the presence of plasma waves where magnetic field oscillation modes can be observed.

7. **Orbital analysis:** GPS ephemeris should be relied upon more heavily relied upon for orbital analysis for the CASSIOPE (observer) satellite as it provides more definitive measurements of position relative to the wake geometry. The secondary objects in a conjunction are less likely to have operator ephemeris (such as debris objects) so increased utilization of CDM messages would benefit data processing if the secondary object ephemeris is unavailable.

8. FUTURE DIRECTION OF RESEARCH

It has been long known that plasma wave noise can be self-generated by LEO spacecraft [15] and interplanetary spacecraft during encounters with the Earth [16]. Recent experimentation has found that thruster bursts from space objects in LEO where a considerable amount of propellant is used can be detected several hundred kilometres from the maneuvering satellite as electric field noise [17]. The sensing of propulsion events would be useful to the SSA community as it would provide direct insight as to whether a satellite was maneuvering at the time of observation. This prevents the necessity of measuring large orbital arcs and determining if orbit determination residuals show evidence of a maneuver. Direct measurements indicating if a satellite thruster was in use can provide immediate insight into the operational state of a satellite.

Formation flight measurements from a small subsatellite performing elliptical relative motion about space shuttle Atlantis in 1988 [15] detected broadband electrostatic noise from both a) within the wake of the shuttle, and b) during intervals where geomagnetic field lines "threaded" the shuttle's wake. This noise was detected at ranges up to several hundred meters from the shuttle. The noise was attributed to currents stimulated by a cloud of water vapor and other particles emitted by the shuttle either venting or maneuvering in space. The noise was also uniquely detected at times when the local magnetic field line "threaded" the wake of the space shuttle even though the subsatellite was clearly outside of the wake region. This suggests that field-aligned waves may be detectable if the noise generation source originated in the wake of the space shuttle.

During the Jupiter-bound Galileo mission's gravity assisted pass by the Earth, its electric field sensor noted periodic pulses in the Lower Hybrid Resonance (~6 kHz) [16] which were found to be attributed to the spin rate of Galileo, and the times that its boom-mounted electric field antenna threaded a magnetic field line with Galileo's own wake. This effect suggests that broadband wave noise generated in the wake of Galileo travelled along magnetic field lines

to its boom-mounted electric field antenna. The LHR was attributed to be the origin of those waves, possibly due to the Lower Hybrid Mode drift instability [16].

Both the findings from the shuttle, and that of Galileo suggest that electrostatic noise propagating relative to the geomagnetic field lines may be another avenue to explore for sensing space objects. Both allude to noise which propagates along the geomagnetic field lines and is suggestive of the lower hybrid mode – a mix of ion and electron gyrofrequencies and the plasma frequency when wave propagation is nearly perpendicular to the magnetic field. While the Starlink 2521 findings were not repeated in this dataset, the geometric conditions of its observation were consistent with these two previous findings. Alternatively, propulsion-related activity cannot be ruled out as propulsion events are known to generate significant electric field perturbations at long distances from spacecraft [17]. Starlinks regularly operate electric propulsion systems so its use, or that of another nearby Starlink operating its thruster cannot be ruled out as a possible source of the wave power.

Current work is now focusing on plasma wave generation mechanisms from charged space objects in LEO. Space objects are predicted to charge slightly negative (~ -0.6 V) and may generate plasma waves which may offer another approach to sense space objects aside from charge density variations. This is now being explored as an alternative means to detect space objects at potentially greater distances, and much more enabling geometries for a space-based observer [18]. A model describing how a moving space object can create plasma waves like the Cherenkov radiation effect is now being worked on.

9. CONCLUSION

CASSIOPE collected space-based observations of the VLF environment during conjunctions between itself and other space objects conjuncting with it. The aim was to detect broadband wave energy provoked by CASSIOPE's rapid traversal of ion density rarefactions in, or near, the ion-acoustic wake of the secondary object. The rigid geometric constraint required for this type of observation, and the generally large separations between CASSIOPE and other space objects during conjunctions yielded limited data suggesting that density rarefactions can be exploited to observe the presence of a space object.

The strongest evidence was demonstrated in one conjunction between Starlink 2571 where CASSIOPE passed below the Starlink, but its wake region was connective to CASSIOPE via the geomagnetic field lines with broadband energy spanning the ion gyrofrequency to the Lower Hybrid Resonance (~6 kHz). Starlink 2672 similarly showed broadband energy near the Lower Hybrid Resonance but was observed ~63 seconds prior to TCA. This suggests it may not have been associated with Starlink 2672 but perhaps another object or electric thrust transients from the Starlink constellation. A conjunction between COSMOS 2251 debris and Iridium 911 showed VLF power enhancement at TCA below 6 kHz but were difficult to separate from natural ionospheric environment effects. All other 31 conjunction observations did not yield low frequency VLF power associated with their TCA.

Detected electric field strengths were in the ~1 mV/m range or less and did not reach anywhere near the ~1 V/m range predicted for a wake traversal. CASSIOPE passages through the far wake (> 6 km) of some space objects (COSMOS 2251 debris, and Iridium 911) showed VLF electric field strengths less than ~1 mV/m.

This work did highlight several geophysical and orbital constraints which could help refine the times to observe conjunctions to assess the viability of detecting space objects by their impact on the plasma environment. Future work will use more rigorous constraints when planning RRI data acquisition respecting the quasi-conical geometry of the wake, space object altitude and the auroral regions. Plasma wave approaches will be examined in the future as an alternative means to detect space objects by searching for plasma oscillations in charged particle current, magnetic or electric field. It is now believed that VLF waves spanning the ion cyclotron frequencies (~0.036 - 2 kHz) to the Lower Hybrid Resonance (~6 kHz) appears to be a key phenomenology of plasma physics for objects moving at high relative velocities in Earth's ionosphere.

10. ACKNOWLEDGEMENTS

11. REFERENCES

[1] Stokes, G.H., von Braun, C., Ramaswamy, S., Harrison, D., Sharma, J., The Space Based Visible Program, Lincoln Lab Journal, Vol.11, No. 2, (1998).

[2] Space Based Space Surveillance (SBSS), eoportal.org, https://www.eoportal.org/satellite-missions/sbss, accessed 17 Aug 2023.

[3] Maskell, P.,Oram, L., Sapphire: Canada's Answer to Space-Based Surveillance of Orbital Objects, AMOS Conference 2008, Maui Economic Development Board, Maui, HI, 2008.

[4] Scott, R.L., Thorsteinson, S.E., Key Findings from the NEOSsat Space-Based SSA Microsatellite Mission", Defence R&D Canada DRDC-RDDC-2018-N166, (2018). Presented at the 2018 AMOS Conference.

[5] ORS-5 (Operationally Responsive Space-5), eoportal.org, https://www.eoportal.org/satellite-missions/ors-5#references, accessed 17 Aug 20203.

[6] Andrew Yau, Gordon James, Gregory Enno, Robert Hum, Peter Duggan, Mark Senez, Ziad Ali, Gilles Brassard, Berthier Desjardins, Luc Dubé, Richard Giroux, Dave Beattie, Ian Walkty, Multidimensional Challenges and Benefits of the CASSIOPE Mission, *Proceedings of the IAA Symposium on Small Satellite Systems and Services* (4S), Rhodes, Greece, May 26-30, 2008, ESA SP-660, August 2008

[7] Al pert, Y.L., Pitaevskii, L.P., *Space Physics with Artificial Satellites*, Springer Science Business Media, New York, (1965).

[8] Hastings, D., Garret, H., *Spacecraft Environment Interactions*, Cambridge University Press, 1996.

[9] James, H.G., King, E.P., White, A., Hum, R.H., Lunscher, W.H.H.L., Siefring., C.L., The e-POP Radio Receiver Instrument on CASSIOPE., *Space Science Rev*, 189:79-105. (2014).

[10] ePOP data page, https://epop-data.phys.ucalgary.ca/, University of Calgary, accessed 18 Aug 2023.

[11] Celestrak SOCRATES, https://celestrak.org/SOCRATES/, Accessed 9 Aug 2023.

[12] 18th and 19th Space Defence Squadron, *Spaceflight Safety Handbook for Satellite Operators*, Version 1.7, April 2023. Accessible from https://www.space-track.org/documents/SFS_Handbook_For_Operators_V1.7.pdf. Accessed 9 Aug 2023.

[13] Hargreaves, J.K., *The solar-terrestrial environment*, Cambridge Atmospheric and Space Sciences, pp74-77, Cambridge University Press, (1992).

[14] SpaceX discussion, private communication regarding Starlink electric propulsion, May 2022.

[15] Gurnett, D.A., Kurth, W.S., Steinberg, J.T., Plasma Wave Turbulence Around the Shuttle: Results from SpaceLab-2 Flight, *Geophysical Research Letters*, Vol. 15, No. 8., pp 760-765, August (1988).

[16] Keller, A.E., Gurnett, A.D. Kurth, W.S., Yuan, Y., Bhattacharjee., A., Lower Hybrid waves generated in the wake of the Galileo Spacecraft, *Planet Space Sci*, Vol 45, No.2., pp 201-219, (1997).

[17] Bernhardt, P.A., Griffin, M.K., Bougras., W.C., Howarth., A.D., James., H.G., Siefring., C.L., Bricinski., S.J., Satellite observations of strong plasma waves emissions from frequency shifts induced by an engine burn from the Cygnus Spacecraft, *Radio Science*, 56, e2020RS007143. (2020).

[18] Bernhardt, P.A., Scott, R.L., Howarth, A., Morales, G., Observations of plasma waves generated by charged space objects, *Physics of Plasmas*, In Press, (2023) DOI: 10.1063/5.0155454.

ANNEX 1 - Secondary objects conjuncting with CASSIOPE in 2022 where RRI data was collected.
Shaded rows indicate conjunctions where some broadband power was observed in the VLF

SSN ID	Object Name	Time of Closest Approach (UTC)	Miss distance (km)	Secondary object altitude (km)	Radial miss (km)	In-track miss distance (km)	Cross-track miss distance (km)	Magnetic latitude (deg)	MLT (hrs)	Sun Cond.	VLF power observed at TCA? / Notes
48650	STARLINK-2672	04 Mar 2022 00:28:12.162	17.73	554.50	1.30	-7.71	-15.91	-29.28,	2.18	Eclipse	TCA - 63s
48648	STARLINK-2521	04 Mar 2022 03:48:43.179	0.24	555.28	0.09	-0.09	-0.20	-21.00,	2.30	Eclipse	At TCA
35671	COSMOS 2251 DEB	27 Mar 2022 08:08:00.326	7.92	782.44	0.16	5.22	5.95	68.87	19.79	Sun	At TCA, auroral noise
24842	IRIDIUM 911	28 Mar 2022 01:37:47.249	7.32	773.07	0.83	7.17	1.19	77.35	10.12	Sun	Auroral noise after TCA
41416	NOAA 16 DEB	06 Apr 2022 04:31:24.390	4.78	839.15	-3.04	-0.54	-3.65	-74.97	1.97	Sun	-
30680	FENGYUN 1C DEB	06 Apr 2022 11:13:12.202	4.01	863.56	-1.23	0.44	3.79	-71.33	5.67	Sun	-
41950	FLOCK 3P 20	06 Apr 2022 21:00:44.617	4.82	482.06	2.82	-0.15	-3.91	-39.97	21.91	Eclipse	-
41064	NOAA 16 DEB	06 Apr 2022 21:14:29.954	2.69	861.43	1.48	0.48	2.19	-89.55	11.42	Sun	-
30237	FENGYUN 1C DEB	07 Apr 2022 08:55:15.654	1.85	838.14	0.17	0.05	1.84	-71.59	3.29	Sun	Data gaps during recording
47520	FLOCK 4S 29	07 Apr 2022 11:35:03.538	4.78	539.13	-4.68	-0.17	-0.93	61.45	20.56	Sun	-
47442	SPACEBEE-63	07 Apr 2022 14:55:43.828	3.81	533.71	3.73	0.14	0.75	-43.06	21.80	Sun	Strong whistlers at TCA
30054	FENGYUN 1C DEB	07 Apr 2022 18:56:50.673	2.53	844.28	1.48	-0.44	2.00	-89.35	5.67	Sun	Auroral noise
48372	STARLINK-2572	08 Apr 2022 23:11:20.270	95.30	576.63	-12.23	-84.71	-41.93	-43.06	21.80	Eclipse	Strong natural whistlers
44084	LEMUR 2	09 Apr 2022 07:28:40.736	7.05	479.87	-2.13	-0.06	-6.73	-29.67	22.23	Eclipse	-
47426	SPACEBEE-46	09 Apr 2022 12:31:41.079	6.15	537.58	-6.09	0.14	-0.85	-48.77	22.31	Eclipse	B-field threads wake, whistlers
29956	FENGYUN 1C DEB	09 Apr 2022 12:44:26.985	8.94	899.11	3.10	-1.58	8.23	-75.0	5.32	Sun	-
25262	IRIDIUM 51	12 Apr 2022 01:47:28.806	11.81	596.97	3.96	-7.38	8.33	73.89	11.33	Sun	-
20510	OKEAN 2	12 Apr 2022 08:28:54.956	8.38	582.04	-7.92	2.14	-1.72	71.67	14.66	Sun	Data gaps in h5 file
48021	STARLINK-2301	12 Apr 2022 09:01:46.299	16.28	563.02	-3.50	-7.84	-13.83	-38.20	21.99	Sun	Whistlers near TCA
22591	SL-8 R/B	12 Apr 2022 09:54:34.915	12.28	970.20	-11.00	-1.26	5.31	37.17	9.85	Sun	Audible voice broadcast?
52111	STARLINK-3708	12 Apr 2022 10:20:35.789	236.10	354.01	-3.84	-210.25	-107.36	40.30	19.96	Sunset	High noise environment
47979	STARLINK-2325	12 Apr 2022 12:22:14.031	16.78	563.64	-4.07	-7.98	-14.19	-44.87	21.73	Eclipse	Heavy whistlers, 20 kHz noise
44820	CZ-4C R/B	12 Apr 2022 15:09:58.807	15.44	576.79	14.90	-0.12	4.03	81.73	17.86	Sun	-
47765	STARLINK-2183	12 Apr 2022 20:24:02.644	189.37	334.10	4.69	95.52	163.45	41.78	21.16	Sunset	Heavy noise at TCA
11060	TIROS N	12 Apr 2022 22:33:16.183	19.02	844.50	7.81	0.00	17.34	-66.03	21.45	Sunrise	Heavy auroral noise
52103	STARLINK-3705	13 Apr 2022 21:26:52.446	350.96	337.65	5.67	-316.93	-150.66	49.18	20.99	Sunset	Audible voice broadcast?
45076	STARLINK-1180	13 Apr 2022 23:26:03.625	15.91	543.80	12.82	-4.62	-8.21	-22.98	21.15	Eclipse	Whistlers at TCA and about
45139	ONEWEB-0026	14 Apr 2022 04:52:03.893	485.27	1175.24	52.37	481.37	31.83	-	-	-	Recording begins 8.5s after TCA
49215	ONEWEB-0351	14 Apr 2022 07:16:51.903	87.17	532.69	77.54	-27.38	28.92	71.49	14.2	Sun	-
51625	ONEWEB-0416	14 Apr 2022 10:25:31.506	89.23	847.38	-60.61	-59.65	27.03	48.58	9.91	Sun	-
49298	ONEWEB-0372	14 Apr 2022 10:36:23.435	60.83	554.85	49.21	-19.88	29.73	74.27	14.99	Sun	-
45348	SL-14 DEB	25 Apr 2022 16:40:59.056	5.44	1198.32	0.36	-1.09	5.32	-40.70	7.29	Sun	No recording at TCA
48055	ONEWEB-0157	30 Apr 2022 05:03:18.579	6.77	1238.80	0.35	-5.99	-3.14	-71.64	1.14	Sun	-
46027	STARLINK-1522	09 Jun 2022 10:47:58.872	3.07	550.59	0.54	1.72	-2.48	48.49	0.96	Sun	-
31126	MAST	10 Jun 2022 04:33:30.934	0.21	668.50	-0.03	-0.02	-0.20	-77.71	19.41	Sun	Electronic noise at TCA